Mon. Not. R. Astron. Soc. **000**, 1–12 (2009) Printed 1 September 2009 (MN LATEX style file v2.2)

Correlated optical/X-ray variability in the high-mass X-ray binary SAX J2103.5+4545

P. Reig[1,2⋆], A. Słowikowska[1,2], A. Zezas[1,2,3] and P. Blay[4]
[1]*IESL, Foundation for Research and Technology, 71110 Heraklion, Crete, Greece*
[2]*University of Crete, Physics Department, PO Box 2208, 710 03 Heraklion, Crete, Greece*
[3] *Harvard-Smithsonian Center for Astrophysics, 60, Garden Street, Cambridge, MA 02138, USA*
[4]*Image Processing Laboratory, University of Valencia, 46071 Paterna-Valencia, Spain*

Accepted ??. Received ??; in original form ??

ABSTRACT

SAX J2103.5+4545 is the Be/X-ray binary with the shortest orbital period. It shows extended bright and faint X-ray states that last for a few hundred days. The main objective of this work is to investigate the relationship between the X-ray and optical variability and to characterise the spectral and timing properties of the bright and faint states. We have found a correlation between the spectral and temporal parameters that fit the energy and power spectra. Softer energy spectra correspond to softer power spectra. That is to say, when the energy spectrum is soft the power at high frequencies is suppressed. We also present the results of our monitoring of the Hα line of the optical counterpart since its discovery in 2003. There is a correlation between the strength and shape of the Hα line, originated in the circumstellar envelope of the massive companion and the X-ray emission from the vicinity of the neutron star. Hα emission, indicative of an equatorial disc around the B-type star, is detected whenever the source is bright in X-rays. When the disc is absent, the X-ray emission decreases significantly. The long-term variability of SAX J2103.5+4545 is characterised by fast episodes of disc loss and subsequent reformation. The time scales for the loss and reformation of the disc (about 2 years) are the fastest among Be/X-ray binaries.

Key words: X-rays: binaries – stars: neutron – stars: binaries close –stars: emission line, Be

1 INTRODUCTION

High-mass X-ray binaries (HMXB) typically consist of a neutron star orbiting around an early-type star. They divide into two major groups according to the luminosity class of the optical component: supergiant X-ray binaries if the massive companion is an evolved star (luminosity class I-II) and Be/X-ray binaries (BeX) if it is a main-sequence or giant star. The vast majority of BeX are transient systems, although there is a small group of persistent sources (Reig & Roche 1999). Transient BeX have orbital periods in the range 20-100 days and spin periods shorter than ∼200 s. In contrast, persistent BeX present orbital periods typically longer than ∼100 days and spin periods longer than ∼200 s. Supergiant X-ray binary systems have narrower orbits with orbital periods shorter than 10 days and contain slow-rotating neutron stars, with spin periods of the order of minutes to hours.

SAX J2103.5+4545 is an unusual HMXB. Its spin, $P_{\rm spin}$ = 358.6 s (Hulleman et al. 1998), and orbital, $P_{\rm orb}$ = 12.7 d (Baykal et al. 2002) periods are typical of supergiant X-ray binaries. In fact, SAX J2103.5+4545 falls in the wind-fed supergiant region (Reig et al. 2004) of the $P_{\rm orb} - P_{\rm spin}$ diagram (Corbet 1986). However, the primary component of the binary is a main-sequence star of spectral type B0 (Reig et al. 2004), i.e. SAX J2103.5+4545 belongs to the BeX category. SAX J2103.5+4545 alternates X-ray bright states that last for a few months with extended (as long as few years) X-ray faint states (Baykal et al. 2002). During the bright states SAX J2103.5+4545 shows large spin-up episodes (Inam et al. 2004; Sidoli et al. 2005), indicating that an accretion disc is formed around the neutron star (Baykal et al. 2002). The scarce optical data seem to suggest that during the bright state the Hα line turns into emission, implying that a decretion circumstellar disc is formed around the Be star (Reig et al. 2004). These discs are probably short lived and appear during the high X-ray emission states only. Reig et al. (2005) found that SAX J2103.5+4545 was emitting X-rays even after the complete loss of the circumstellar disc. They argue that in this state the X-rays are the result of wind-fed accretion.

Since the discovery of SAX J2103.5+4545 in February 1997, the system has been observed in the X-ray band on numerous occasions. The first X-ray observations were made with *BeppoSAX* (Hulleman et al. 1998). The source was active for about eight months and reached a peak intensity of 20 mCrab (2–25 keV) on

⋆ E-mail: pau@physics.uoc.gr

[h]

Table 1. Hα equivalent width measurements (1σ errors). See Fig. 3 for a representative example of the line profiles.

Date	Julian date (2,400,000+)	EW(Hα) (Å)	Hα profile[a]	Telescope
01/08/2003	52853.5	-2.14±0.16	DPE	SKI
17/08/2003	52869.6	-1.06±0.09	SH	WHT
14/09/2003	52897.3	+2.51±0.11	ABS	WHT
06/10/2003	52919.3	+2.31±0.16	ABS	SKI
08/10/2003	52921.3	+2.08±0.12	CQE	SKI
03/12/2003	52977.3	+2.11±0.31	ABS	CAL
23/05/2004	53149.6	+2.61±0.24	CQE	SKI
27/05/2004	53153.6	+2.61±0.34	CQE	SKI
28/05/2004	53154.5	+2.50±0.19	CQE	SKI
23/06/2003	53180.5	+1.90±0.08	CQE	SKI
25/06/2004	53182.5	+2.39±0.27	ABS	SKI
07/07/2004	53194.5	+2.80±0.17	ABS	SKI
25/08/2004	53243.5	+2.34±0.15	CQE	SKI
26/08/2004	53244.4	+2.15±0.12	CQE	SKI
27/08/2004	53245.4	+1.93±0.10	CQE	SKI
01/09/2004	53250.6	+2.33±0.11	ABS	WHT
03/09/2004	53252.5	+2.30±0.13	ABS	SKI
12/09/3004	53261.4	+2.16±0.07	ABS	SKI
13/09/2004	53262.3	+2.11±0.18	ABS	SKI
25/10/2004	53304.3	+2.49±0.31	CQE	SKI
23/06/2005	53545.4	+2.31±0.13	CQE	SKI
11/07/2005	53563.5	+2.59±0.11	ABS	SKI
29/07/2005	53581.4	+2.46±0.10	ABS	SKI
16/08/2005	53599.5	+2.27±0.08	ABS	SKI
20/09/2005	53634.4	+2.35±0.06	ABS	SKI
26/10/2005	53670.4	+1.21±0.05	CQE	SKI
20/06/2006	53907.5	+2.43±0.11	ABS	SKI
03/10/2006	54012.3	+1.98±0.12	CQE	SKI
14/05/2007	54235.4	-2.29±0.24	DPE	SKI
20/05/2007	54241.4	-1.72±0.21	DPE	SKI
29/05/2007	54250.5	-1.58±0.09	DPE	SKI
09/06/2007	54261.9	-1.19±0.11	DPE	FLW
22/06/2007	54274.9	-1.06±0.14	DPE	FLW
04/09/2007	54348.5	-5.02±0.31	DPE	SKI
06/09/2007	54350.5	-4.18±0.32	DPE	SKI
09/09/2007	54353.5	-5.12±0.41	DPE	SKI
11/09/2007	54355.4	-4.88±0.24	DPE	SKI
14/09/2007	54358.9	-4.35±0.28	DPE	FLW
02/10/2007	54376.3	-4.65±0.36	DPE	SKI
03/10/2007	54377.3	-4.24±0.41	DPE	SKI
05/12/2007	54439.6	-1.00±0.10	SH	FWL
24/06/2008	54642.4	+2.02±0.09	CQE	SKI
25/06/2008	54643.4	+2.18±0.14	CQE	SKI
14/07/2008	54662.4	+2.21±0.10	CQE	SKI
08/08/2008	54687.4	+2.33±0.08	CQE	SKI
12/08/2008	54691.3	+1.93±0.17	ABS	SKI
02/09/2008	54712.3	+2.26±0.04	CQE	SKI
08/05/2009	54960.5	+2.10±0.13	CQE	SKI
17/05/2009	54969.5	+2.03±0.13	ABS	SKI
27/05/2009	54979.6	+2.16±0.11	ABS	SKI

a: ABS: absorption, CQE: absorption with central quasi-emission peak DPE: double-peak emission, SH: shell profile.

April 11, 1997. The X-ray emission showed pulsations with a period of 358.61 s.

The All Sky Monitor on board *RXTE* detected a second bright state two years later (Baykal et al. 2000), reaching a peak intensity of 27 mCrab (2-12 keV) on October 28, 1999. The continuous monitoring of SAX J2103.5+4545 by *RXTE* and *INTEGRAL* since July 2002 allowed detailed pulse frequency analysis and the determination of the orbital parameters (Baykal et al. 2007; Camero-Arranz et al. 2007): the system has a moderately eccentric orbit with $e = 0.401 \pm 0.018$, an orbital period of 12.66528 ± 0.00051 days, and a semi-major axis of 80.8 ± 0.7 lt-s.

In addition to *BeppoSAX* and *RXTE*, SAX J2103.5+4545 has been observed with *XMM-Newton* and *INTEGRAL* in the bright state, hence allowing the characterisation of the energy spectrum from 0.1 to 150 keV. At low energies (< 4 keV), the X-ray energy spectrum presents a soft spectral component, consistent with blackbody emission with $kT = 1.9$ keV and emitting radius of ~0.3 km (Inam et al. 2004). The broad-band (4-150 keV) energy spectrum is well fitted by a power-law ($\Gamma = 1 - 1.5$) with an exponential cutoff ($E_{\rm cut} = 8 - 19$ keV), and with a Kα fluorescence emission line (~6.4 keV) from cool iron (Blay et al. 2004; Sidoli et al. 2005).

The spectral analysis of RXTE data performed by Baykal et al. (2002) covering the interval November 1999–August 2000 indicate that the spectrum of SAX J2103.5+4545 is harder during bright states. This result was confirmed by the X-ray colour analysis performed by Camero-Arranz et al. (2007) using six years worth of RXTE data. Transient quasi-periodic oscillations around 0.044 Hz have been reported by Inam et al. (2004).

The excellent monitoring of SAX J2103.5+4545 in the X-ray band contrasts with the scarcity of data at other wavelengths. The only published optical/near-IR observations of SAX J2103.5+4545 are those reported by Reig et al. (2004). They identified the optical counterpart with a moderately reddened V=14.2 B0V star, at a distance of 6.5 kpc. In this paper we present the results of our monitoring of the Hα line for the 2003-2009 interval and investigate the X-ray variability of SAX J2103.5+4545 in correlation with the optical data. X-rays result from accretion of matter from the optical companion's circumstellar disc onto the neutron star surface, hence providing information about the physical conditions in the vicinity the compact object. The Hα line is formed in the Be star's disc as reprocessed radiation from its photosphere. Since the disc constitutes the reservoir of matter available for accretion a correlated X-ray/optical study is the best way to unveil the nature of the variability in this system.

2 OBSERVATIONS AND DATA ANALYSIS

2.1 Optical spectra

We have been observing SAX J2103.5+4545 regularly since the identification of the optical counterpart in 2003. We have analysed all available optical observations including those already published by Reig et al. (2004). The new optical spectroscopic observations were obtained mainly from two sites: the Skinakas (SKI) observatory in Crete (Greece) and from the Fred Lawrence Whipple (FLW) observatory at Mt. Hopkins (Arizona). In addition, SAX J2103.5+4545 was observed in service time from the William Herschel Telescope (WHT) at the observatory of El Roque de los Muchachos in La Palma (Spain) on 1 September 2004. One more spectrum was made from the 2.2-m telescope at the observatory of

Table 2. Optical photometric observations of SAX J2103.5+4545.

Date	Julian Date 2,400,000+	B mag	V mag	R mag	I mag
08-06-2003	52799.467	15.35±0.03	14.22±0.02	13.48±0.02	–
24-08-2003	52876.408	15.36±0.02	14.25±0.03	13.57±0.03	12.85±0.03
20-05-2004	53146.558	15.41±0.01	14.32±0.01	13.63±0.01	12.87±0.01
05-07-2004	53192.354	15.42±0.02	14.33±0.01	13.64±0.02	12.92±0.02
24-08-2004	53242.477	15.39±0.02	14.31±0.01	13.61±0.01	12.85±0.02
14-09-2004	53263.375	15.39±0.02	14.27±0.02	13.58±0.01	12.84±0.03
01-10-2004	53280.370	15.41±0.02	14.31±0.02	13.61±0.02	12.86±0.02
26-06-2005	53548.497	15.39±0.02	14.30±0.01	13.61±0.02	12.86±0.04
27-07-2005	53579.502	15.38±0.02	14.29±0.01	13.60±0.01	–
20-08-2005	53603.414	15.42±0.02	14.35±0.03	13.66±0.02	–
18-08-2006	53966.519	15.42±0.03	14.32±0.03	13.63±0.02	–
16-07-2007	54298.493	15.12±0.03	13.75±0.03	12.93±0.03	12.05±0.03
01-09-2007	54345.426	15.21±0.03	13.94±0.02	13.15±0.03	12.32±0.04
02-09-2007	54346.496	15.12±0.03	13.89±0.03	13.11±0.02	12.28±0.02
26-10-2007	54400.242	15.37±0.03	14.21±0.03	13.57±0.04	12.78±0.05
05-08-2008	54684.434	15.41±0.02	14.29±0.02	13.60±0.02	12.87±0.02

Calar Alto (CAL) in Almería (Spain) on 3 December 2003. Table 1 gives the log of the spectroscopic observations and the value of the Hα equivalent width.

The 1.3 m telescope of the Skinakas Observatory was equipped with a 2000×800 (15 μm) pixel ISA SITe CCD and a 1302 l mm^{-1} grating, giving a nominal dispersion of ∼1 Å/pixel. The instrumental set-up during the service WHT observation consisted of the ISIS spectrograph with the R1200R grating, giving a dispersion of 0.23 Å/pixel and covering the wavelength interval between 6040–6900 Å. The spectrum was obtained with the 4096×2048 (13.5 μm) pixels MARCONI2 CCD. The reduction of these spectra was made using the STARLINK *Figaro* and IRAF v2.14 packages, while their analysis was performed using the STARLINK *Dipso* package. The FLW observations of SAX J2103.5+4545 were made in queue mode with the 1.5-m telescope and the FAST-II spectrograph (Fabricant et al. 1998). Three observations were obtained with the 1200 l mm^{-1} grating and one observation (5 December 2007) with the 600 l mm^{-1} grating. The tilt of the grating was selected in order to cover the Hα line. The data were analysed with the RoadRunner package (Tokarz & Roll 1997) implemented in IRAF. Spectra of comparison lamps were taken before each exposure in order to account for small variations of the wavelength calibration during the night.

The field around SAX J2103.5+4545 was observed through the Johnson *B*, *V*, *R*, and *I* filters from the 1.3 m telescope of the Skinakas observatory. Observations obtained before July 2007 were performed using a 1024 × 1024 SITe CCD chip with a 24 μm pixel size (corresponding to 0.5″ on sky). From July 2007 a 2048×2048 ANDOR CCD with a 13.5 μm pixel size was used (corresponding to 0.28″ on sky). Standard stars from the Landolt list (Landolt 2009) were used for the photometric calibrations and transformation equations. Reduction of the data was carried out in the standard way using the IRAF tools for aperture photometry.

2.2 X/γ-ray observations

We have analysed all archived observations of SAX J2103.5+4545 made by *RXTE*/PCA and *INTEGRAL*/ISGRI. The *RXTE*/PCA consists of five Proportional Counter Units (PCU), which are sensitive to X-rays in the 2-60 keV energy range (Jahoda et al. 1996). The INTEGRAL Soft Gamma Ray Imager (ISGRI) is the lower energy detector of the Imager on Board INTEGRAL Satellite (IBIS) and operates in the 15–1000 keV energy range (Lebrum et al. 2003).

Table 3. Summary of the RXTE observations.

Proposal ID	MJD start	On-source time (ks)	$< I_x >^a$ cs^{-1}	rms^b (%)
P40125	51501.1846	148.05	20.1	54
P40438	51559.9448	89.79	24.3	57
P50095	51606.2713	154.16	21.4	79
P50417	51764.0044	60.35	7.0	40
P60409	52019.0087	5.20	24.1	41
P70082	52439.9567	446.51	33.2	71
P90097	53029.1948	252.86	9.94	67
P92436	54221.0628	27.98	40.54	86

a: 2-60 keV PCU2 background-subtracted. Time bin: 16 s
b: root-mean-square: standard deviation over the mean intensity

In addition, data from two all sky monitors, namely the All-Sky Monitor (ASM) onboard *RXTE* (Levine et al. 1996) and the Burst Alert Telescope (BAT) onboard *SWIFT* (Barthelmy 2000) have been used to study the long-term variability of SAX J2103.5+4545 (Fig. 1). These two instruments produce daily flux averages in the energy range 1.3-12.1 keV and 15-150 keV, respectively.

RXTE/PCA data can be collected and telemetered to the ground in many different ways depending on the intensity of the source and the spectral and timing resolution desired. In this work we used the two standard modes: *Standard1* provides 0.125-s resolution and no energy resolution; in the *Standard2* configuration data are accumulated every 16 seconds in 129 channels. For the timing analysis *GoodXenon* data, providing maximum spectral (256 channels) and temporal (2^{-20} s) resolution, have also been employed. The number of active proportional counter units varied during the observations. However, PCU2 was always on. To avoid

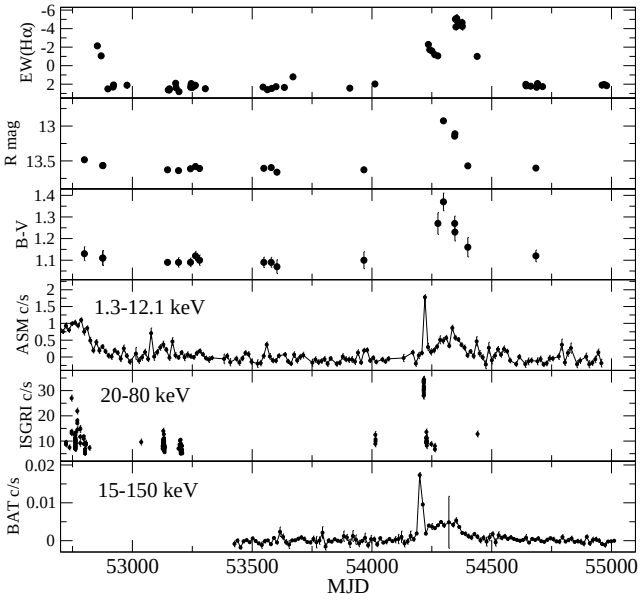

Figure 1. Long-term evolution of the Hα equivalent width, R band and $B-V$ colour. Also shown is the long-term variability in three X-ray bands, corresponding to the *RXTE*/ASM, *INTEGRAL*/ISGRI and *SWIFT*/BAT light curves.

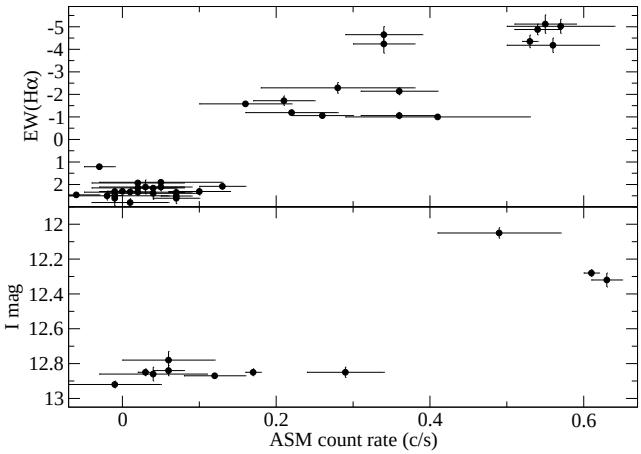

Figure 2. EW(Hα) and I-band magnitude as a function of ASM intensity.

complications with the different response of the each unit and the varying number of active detectors we used PCU2 data for the spectral analysis. Note that the power spectral analysis is not affected by the number of active units as we used the *rms* normalisation (Belloni & Hasinger 1990; Miyamoto et al. 1991), where the power is normalised to the mean intensity of short (128 s) segments. Table 3 gives a log of the *RXTE* observations.

A total of 3513 public data pointings of INTEGRAL included SAX J2103.5+4545 in the IBIS/ISGRI field of view. However, only in 269 the source was detected with significance greater than 3σ above the noise level (detection level greater than 7 based on the standard Offline Scientific Analysis (OSA) software[1]), while in 1436 additional observations we obtained marginal or non reliable detections. In the remaining 1808 pointings the source was below the sensitivity level of IBIS/ISGRI.

OSA version 7.0 have been used to perform light curve and spectra extraction for each science window. To obtain average spectra corresponding to several science windows we used an alternative event extraction method developed by Ferrigno et al. (2007).

3 RESULTS

3.1 Optical photometry

Figure 1 shows the evolution of the Hα equivalent width (EW(Hα)), R-band magnitude and the $B-V$ colour together with the long-term X-ray variability in three different energy bands. Despite the observational gaps in the optical data a correspondence between the variability in the optical band and the X-ray intensity is apparent. Bright X-ray states correspond to enhanced optical activity, both in the photometric magnitudes and colours and the strength of the Hα. This correlation is more clearly seen in Fig. 2, where the EW(Hα) and I-band magnitude as a function of ASM intensity is displayed.

As expected (Dougherty et al. 1994, and references therein), the contribution of the Be star's disc to the photometric magnitudes increases with wavelength. As can be deduced from Table 2, the amplitude of variability of the optical magnitudes between maximum and minimum brightness is 0.3 mag in the B band, 0.6 mag in the V band, 0.7 mag in the R band and 0.8 mag in the I band.

In Reig et al. (2004) values of the reddening and distance were derived from the spectra and the photometric observations. Since *i)* a much longer set of optical photometric observations is now available and *ii)* a longer extended low optical state is observed, where presumably the underlying B star is exposed and photospheric emission without substantial contribution from the disc is detected, it is justified to revisit these values. The main source of uncertainty in estimating the distance stems from the uncertainty of the intrinsic colours and absolute magnitudes associated to each spectral and luminosity class. Difference between different calibrations may amount up to 1.5 mag in the values of the absolute magnitude (Wegner 2006), while differences of 0.04 mag in intrinsic $(B-V)_0$ are found in studies from different authors (Johnson 1966; Wegner 1994). Jaschek & Gómez (1998) analysed the absolute magnitude of about one hundred MK standards and concluded that the intrinsic dispersion of the mean absolute magnitude amounts to 0.7 mag. We have adopted this value as the error on the absolute magnitude.

To estimate the distance to SAX J2103.5+4545 we use the observations showing the bluest colours (those from 20 August 2005, MJD 53603), as no contribution from the circumstellar disc is expected. By comparing the observed colour $(B-V) = 1.07 \pm 0.03$ with the expected one of a B0V star $(B-V)_0 = -0.28$ (Johnson 1966; Gutiérrez-Moreno 1979; Wegner 1994), we derive a colour excess of $E(B-V) = 1.35 \pm 0.03$. Taking the standard reddening law $A_V = (3.1 \pm 0.1)E(B-V)$ and assuming an average absolute magnitude for a B0V star of $M_V = -4.0 \pm 0.7$ (Vacca et al. 1996; Wegner 2006) the distance to SAX J2103.5+4545 is estimated to be $\sim 6.8 \pm 2.3$ kpc. The final error was obtained by propagating the errors of $(B-V)$ (0.03 amg), A_V (0.17 mag) and M_V (0.7 mag). The estimated distance is consistent with the value of 4.5±0.5 kpc derived from the relationship between the pulse frequency derivative and the X-ray flux (Baykal et al. 2007).

[1] The OSA software generates sky images and searches for significant sources. A source is considered as detected if it has a detection level greater than 7, which is equivalent to the classical 3σ level above the measured noise.

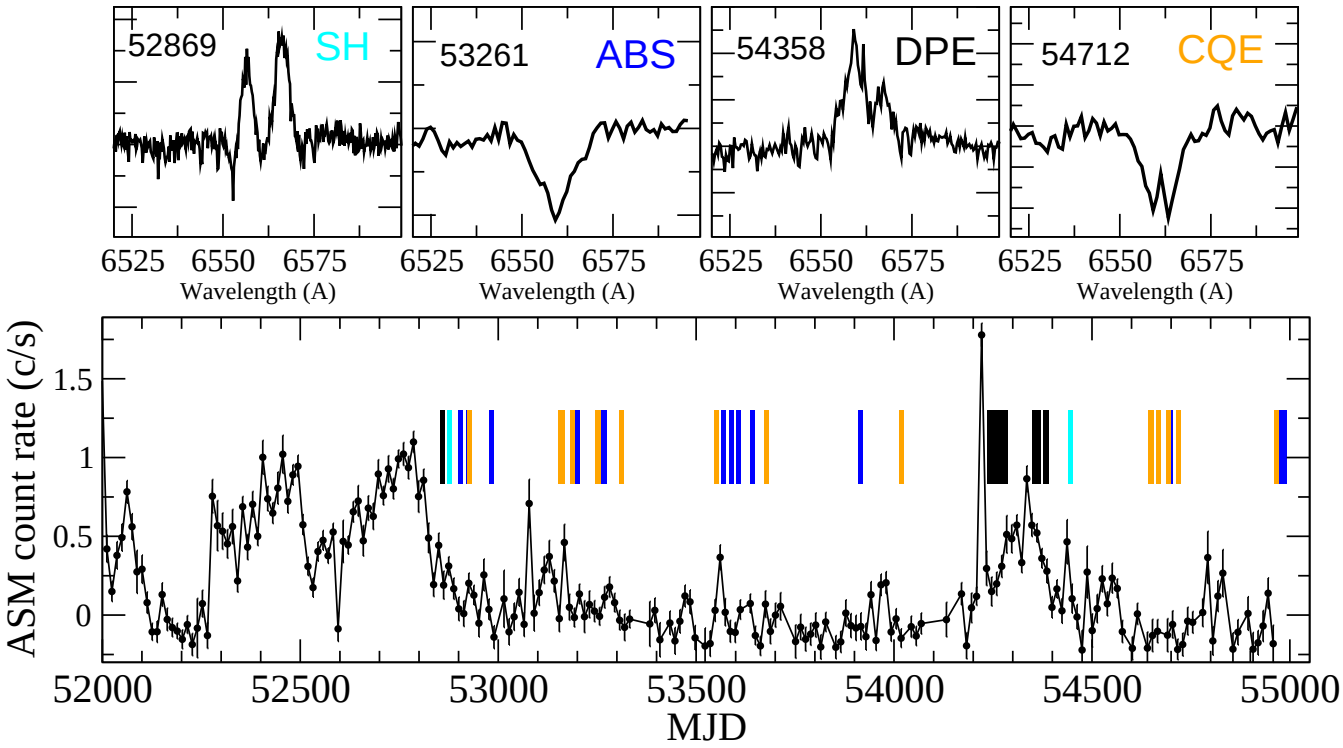

Figure 3. Hα line profiles at different X-ray activity states. *black*: emission (DPE), *blue*: absorption (ABS), *orange*: central quasi-emission (CQE) and *cyan*: shell profiles (SH). Hα emission occurs when the source is X-ray active. *See the electronic edition of the Journal for a colour version of this figure*

.

3.2 Hα line profiles

The monitoring of SAX J2103.5+4545 in the optical band reveals that the Hα line is highly variable, both in strength and shape. In Be stars, the strength and shape of the Hα line provide information about the physical conditions in the circumstellar disc. The measurements of the EW(Hα) are given in Table 1. A negative value indicates that the line appears in emission. The fourth column of Table 1 indicates the profile of the line. We have observed four different profiles (see Fig. 3): emission with a shell profile (SH), absorption (ABS), emission with a split profile (DPE) and central (quasi)-emission peak (CQE). The difference between double-peak profile and a shell profile is simply that in the latter the depression between the two peaks extends below the stellar continuum. CQE is a type of absorption line profile in which the central part of the line core exhibits a weak local flux maximum (Rivinus et al. 1999).

What determines whether the Hα line appears in absorption or emission is the presence of an equatorially concentrated circumstellar disc around the Be star. The absorption lines are formed in the photosphere of the star (i.e., no disc is present) while the emission profile is the result of recombination radiation from ionised hydrogen in the hot, extended circumstellar envelope surrounding the central Be star. CQEs appear when the innermost regions of the disc are being supplied with matter. The deep central absorption in a shell profile is merely due to self-absorption in the envelope as a consequence of a high inclination angle (see e.g. Hanuschik 1995). CQE and shell features are related phenomena. CQEs occur only when shell lines are also present and the lines showing CQE profiles are those also showing a shell feature. Figure 3 show a representative example of each one of these line profiles.

During the bright states, the Hα line exhibits an emission profile, indicating the presence of a circumstellar disc, whereas during the faint states the source shows a purely photospheric absorption profile or a CQE-type profile.

3.3 X-ray states

The long-term X-ray variability of SAX J2103.5+4545 is characterised by bright and faint states (Fig. 4). The bright states appear as outbursts that last typically for 15-20 orbital cycles, i.e. a few hundred of days. These outbursts do not occur in a predictable manner but they do show a general repeatable pattern with regard to the duration and profile of the outburst. In general the outburst begins with a sharp flare that last for one or two orbital periods. This flare is followed by a progressive increase in the X-ray intensity until a maximum is reached at about one order of magnitude above the quiescent level. Assuming an absorbed power-law with exponential cutoff (see below) and a distance of 6.8 kpc, the X-ray luminosity at the peak of the outbursts ranges between $0.6 - 1.0 \times 10^{37}$ erg s^{-1}, while at the peak of the flare the luminosity is typically a factor of 2 higher. During the bright state a modulation of the X-ray intensity with orbital phase is clearly seen (Fig. 4), but it is not detected in the faint state. The average intensity level of the faint state is ~ 5 c s^{-1} PCU^{-1}, which corresponds to a X-ray luminosity of 3.3×10^{35} erg s^{-1} in the 3-30 keV range. Although the count rate may go down to ~ 1 c s^{-1} PCU^{-1} in the faint state, the source is detected in all PCA pointings.

In order to characterise the spectral and timing properties of the source at different states, we selected two subsets of PCA data corresponding to the bright state and two to the faint state. Our selection was based on the source activity, i.e. its PCA flux, and pulsar spin-up rate (see Fig. 12 in Camero-Arranz et al. 2007). During the faint state the spin-up rate is close to zero (or even negative),

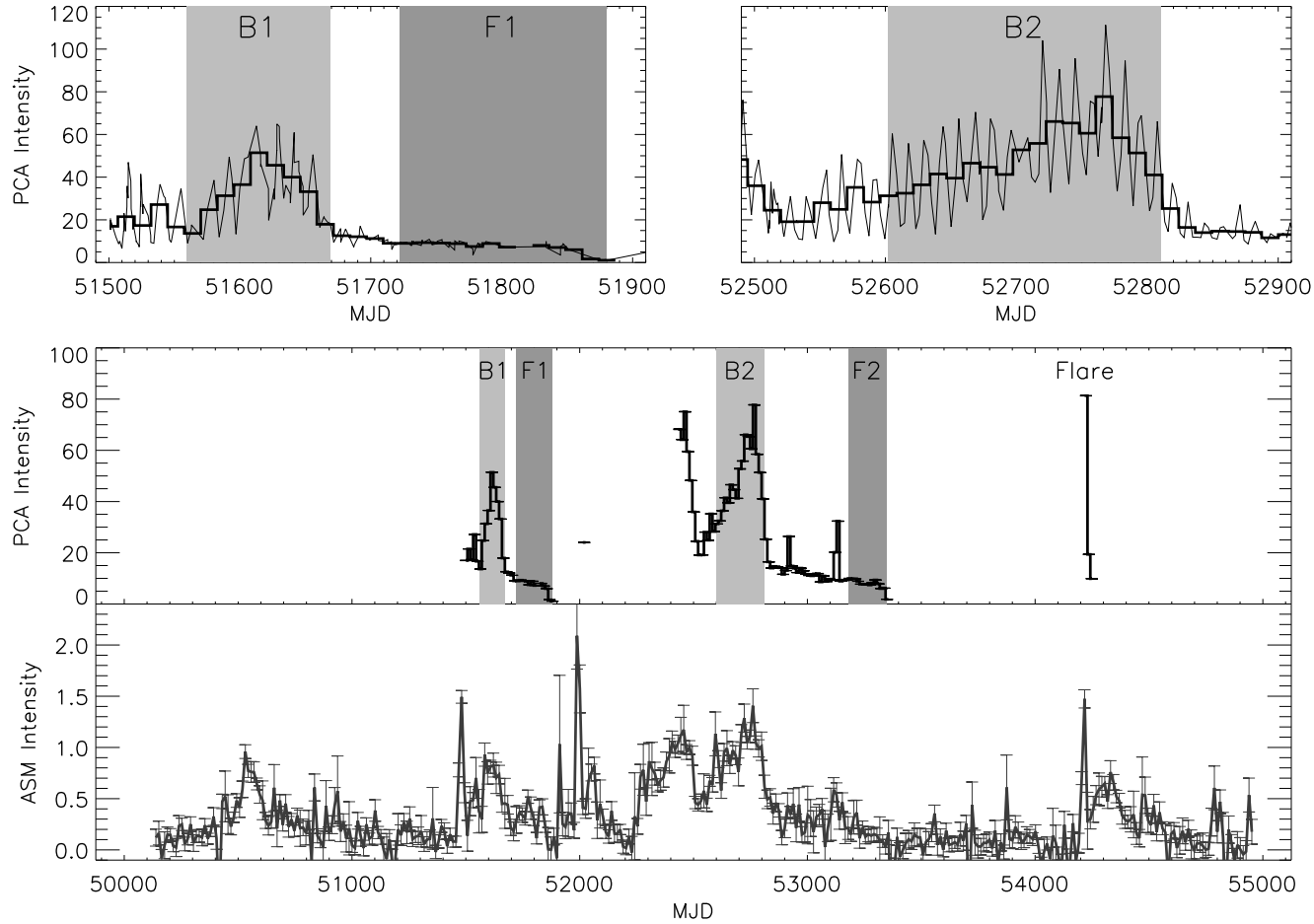

Figure 4. *Bottom panel*: *RXTE*/ASM light curve (1.3-12.1 keV) since April 1996. A bin size equal to the orbital period, $P_{\rm orb}$ = 12.67 d is used. *Middle panel*: *RXTE*/PCU2 (2-60 keV) light curve showing bright (B1, B2) and faint states (F1, F2). *Top panel*: Detailed view of the PCU2 light curve. The 12.7-d binned PCA light curves is superposed on the average count rate per observation interval (typically, a few thousand seconds integration time). Note the modulation of the X-ray intensity with the orbital period during the bright states and the lack of it during the faint state.

whereas during the bright state it is $\gtrsim 2 \times 10^{-13}$ Hz s^{-1}. Thus, faint states correspond to epochs of little or no mass accretion rate. The duration (typically 8–10 orbital periods) of the states was chosen such that it includes the rising and declining phase of the bright state and provides good statistics for the faint state. The time ranges of these intervals are given in Table 4 in Modified Julian Date (MJD), below the state names. Additionally, we selected a one-day subset of PCA data during the flare at MJD 54221 (Fig. 4). Note, however, that RXTE/PCA observations were triggered by the sudden increase of the SAX J2103.5+4545 flux in the ASM light curve. Therefore, the PCA observations did not catch the peak of this flare but began when the flux was already in the declining phase. For each one of these states an average energy spectrum was obtained. A systematic error of 0.6% was added in quadrature to the statistical error in the average energy spectra.

An absorbed power law with a high-energy cut off and an iron line at $\sim$ 6.4 keV provided good fits to all energy spectra in the range 3-30 keV. The spectra of the bright state are distinctly harder than those of the faint state, in agreement with previous findings (Baykal et al. 2002; Camero-Arranz et al. 2007). The cutoff energy in the faint states occurs at slightly higher energies than in the bright state, whereas the central energy of the iron line is slightly larger in the faint state. The line width, however, is not well constrained. If let as a free parameter then the line is broader in the faint state. However, equally good fits are obtained in a relatively wide range of values (σ = 0.3 – 1.0 keV) if this parameter is fixed in the faint state. While the addition of an edge at ∼9 keV clearly improves the fit in the bright state[2], no such edge is required for the faint state. The value of the best-fit parameters of the flare spectrum agree with those of the bright state within the errors.

We also obtained an *INTEGRAL*/IBIS average energy spectrum for the bright2 and faint2 states covering the energy range 20-100 keV. We selected science windows where a statistically significant detection of SAX J2103.5+4545 was found and in which the source lied within 12° off the centre. This radius includes all observations in which the source was within the PCFOV but it disregards the observations in which the source was too close to the detector edge. Figure 5 shows the joint average PCA+ISGRI spectra corresponding to the flare, bright and faint states. To fit these spectra we used the same model as for the PCA data simply adding one extra cutoff power law and a relative normalisation factor (fixed to 1 for the PCA spectrum). However, we fixed the photon index of

[2] The probability that the improvement of the fit in the bright state occurs by chance by the addition of this component is $\lesssim 10^{-3}$ based on the F-test.

Table 4. Spectral parameters resulting from the fits to the *RXTE*/PCA alone and *RXTE*/PCA+*INTEGRAL*/ISGRI energy spectra. Errors denote 90% confidence.

Parameter	Bright1 51559–51669	Bright2 52602–52810	Faint1 51722–51880	Faint2 53180–53348	Flare 54221
			RXTE/PCA energy spectra		
$N_{\rm H}^a$	3.7±0.5	3.7±0.4	4.6±0.9	3.8±0.8	2±1
Photon index	0.85±0.05	0.81±0.02	1.26±0.06	1.21±0.06	0.7±0.1
$E_{\rm cut}$ (keV)	$13.9^{+0.9}_{-0.2}$	13.7±0.3	18±2	18±2	15±2
PL norm^b	$2.30^{+0.09}_{-0.04}$	$3.6^{+0.09}_{-0.06}$	1.07±0.04	1.34±0.08	5.4±0.9
$E_{\rm Fe}$ (keV)	6.44±0.08	6.46±0.08	6.8±0.2	6.6±0.1	6.4±0.2
$\sigma_{\rm Fe}$ (keV)	0.5±0.2	0.4±0.1	0.6^f	0.6^f	0.4^f
EW(Fe) (eV)	160±30	120±20	180±60	160±50	110±60
$E_{\rm edge}$ (keV)	9.7±0.4	9.7±0.4	–	–	–
τ	0.05±0.01	0.05±0.01	–	–	–
Flux^c (3-30 keV)	4.8	8.0	1.0	1.5	18.2
χ^2_r/dof	1.5/45	1.2/45	0.8/47	0.6/47	1.1/47
			INTEGRAL/ISGRI + *RXTE*/PCA energy spectra**		
Photon index	–	0.81^f	–	1.21^f	0.7^f
$E_{\rm cut}$ (keV)	–	21±1	–	19±4	22±1
PL norm^b	–	1.5±0.9	–	0.2±0.2	0.7±0.3
Flux^c (2-100 keV)	–	10.7	–	1.9	27.1
χ^2_r/dof	–	1.1/63	–	0.7/62	1.1/62
			Power spectra		
Power-law index	1.7±0.1	1.6±0.1	2.1±0.4	2.2±0.4	1.39±0.05
rms (%) (0.01-1 Hz)	24±3	25±3	18±5	18±4	25±1

**: It includes the model to the *RXTE*/PCA spectra with the same value of the parameters
a: $\times 10^{22}$ cm^{-2} *c*: $\times 10^{-10}$ erg cm^{-2} s^{-1}
b: $\times 10^{-2}$ cm^{-2} s^{-1} keV^{-1} at 1 keV *f*: fixed

this new component to the best-fit value found in the fit to the PCA data and allow only the cutoff energy and normalisation to vary. In the faint state the addition of *INTEGRAL* data to the PCA fit represents a continuation of the lower energy spectrum, that is, the two cutoff energies are consistent within the errors. In contrast, the broad-band spectra for the bright and flare state are not well fitted by a single power law plus cutoff energy. The extension of the spectra above 30 keV for these two states requires an extra cutoff energy. Table 4 shows the results of the spectral fits. The parameters that fit the PCA spectra also fit the PCA+INTEGRAL spectra. The only difference is the extra exponential decay component.

The large effective area of the *RXTE* instruments make it especially valuable for timing analysis of intensity variations from high-energy sources. Therefore the study of the aperiodic variability of SAX J2103.5+4545 was performed with PCA data only. Given the large number of observations and in order to obtain an homogeneous set of power spectra in terms of energy and frequency range coverage we used the configuration mode *Standard 1*. The light curve corresponding to each PCA observation was binned with bin size 0.125 s, which is the maximum resolution provided by the *Standard 1* data mode, and divided into segments of 128 s. An FFT was calculated for each segment giving power spectra covering the frequency range 1/128–4 Hz. The final power spectrum for each observing interval resulted after averaging all the individual power spectra and logarithmically rebinning in frequency (Fig. 6). In general, the power spectra were well fitted to a single power law. The values of the power-law index and fractional amplitude of variability (*rms*) given in Table 4 correspond to the mean and standard deviation of the average values from all the intervals included in each state. Given the intrinsic variability of the source, we preferred to obtain mean values from the relevant observations rather than one single average power spectrum from the entire light curve of each state . Intervals resulting with less than six segments (i.e. six power spectra) were not considered because of poor statistics (low number of points in the low-frequency bins). Likewise, power spectra whose fits to a power law gave reduced χ^2 larger than 2 were rejected. Since the flare state include one only observational interval the values quoted are those from the average power spectrum of that interval. From the results shown in Table 4 we conclude that the red noise component becomes flatter as the X-ray flux increases.

3.4 X-ray spectral-temporal correlation in the bright state

In addition to characterising the bright and faint states we also searched for correlations between the temporal and spectral parameters on shorter timescales. For each PCA observation falling in one of the two bright or two faint states defined above we obtained an energy spectrum and two power spectra corresponding to the energy ranges 3–10 keV, 10–30 keV, respectively. In this case the light curve at different energies were extracted from data of the *GoodXenon* configuration mode. As before, the 3–30 keV energy spectra were fitted with an absorbed power law plus exponential cutoff and a Gaussian representing fluorescence from cold iron,

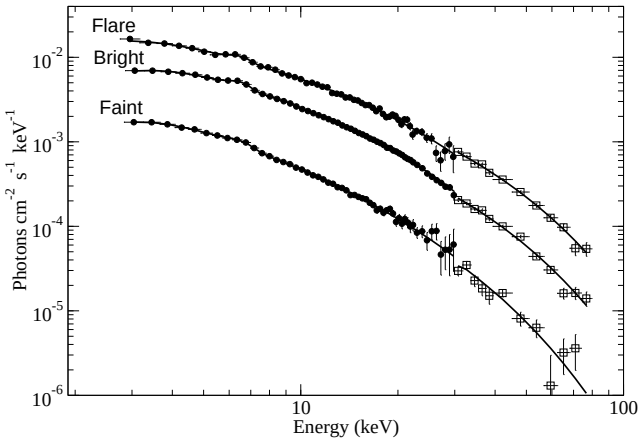

Figure 5. Joint PCA+ISGRI spectra for the flare, bright2 and faint2 states. The model components comprises two cutoff power laws, a Gaussian and low-energy absorption. Circles correspond to PCA data and squares to ISGRI data.

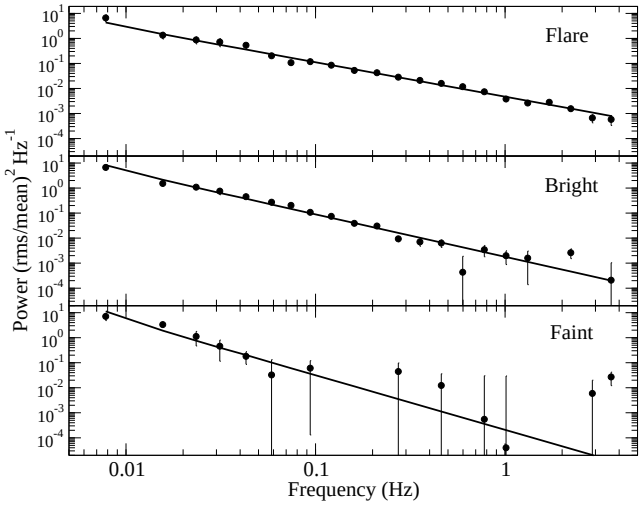

Figure 6. Power spectra for the flare (MJD 54221), bright2 (MJD 52653) and faint2 (MJD 53265) states.

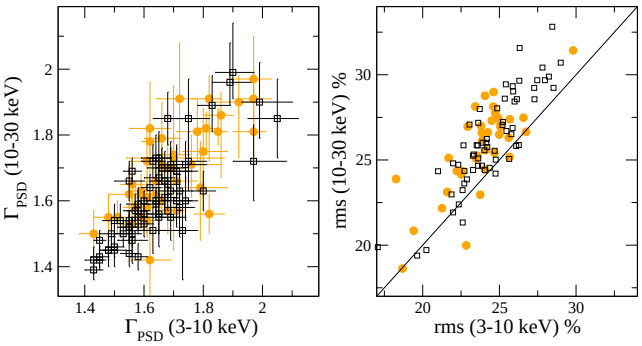

Figure 7. Relationship between the power-law index and *rms* resulting from the fits to the power spectra in two energy bands for the two bright states. Circles represent state 1 and squares correspond to state 2.

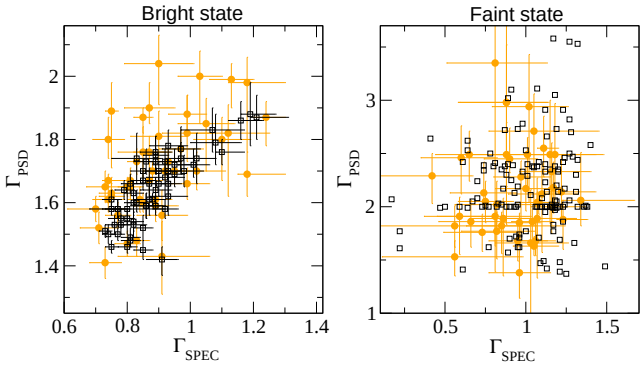

Figure 8. The $\Gamma_{SPEC}-\Gamma_{PSD}$ diagram. Slope of the power spectral continuum as a function of the photon index of the energy spectrum. Circles represent state 1 and squares state 2. For clarity the error bars of the faint2 state were omitted.

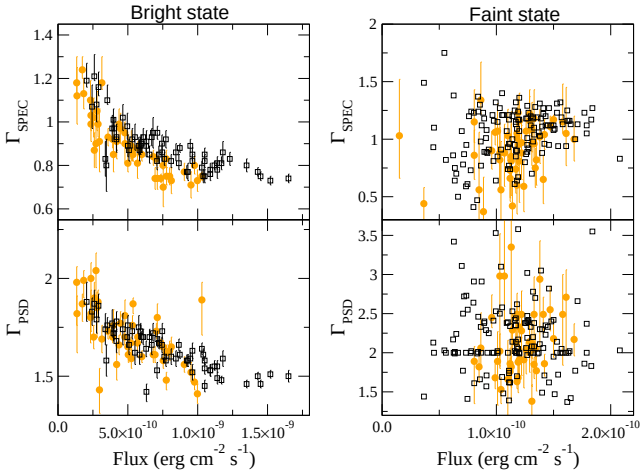

Figure 9. Photon index and power-law index as a function of X-ray flux in the 3-30 keV range. Circles represent state 1, while squares correspond to state 2. For clarity the error bars of the faint2 state were omitted.

while the power spectra exhibited strong red noise that was fitted with a single power law.

We first checked whether the aperiodic variability, i.e., the continuum of the power spectra, depended on energy. Fig. 7 shows the power-law index obtained from the 3-10 keV and 10-30 keV power spectra for the bright states. A fit of both sets of data to a straight line gives a slope of 0.83±0.06, indicating that the power spectral continuum weakly depends on energy. That is, on average, the slope of the power spectra at higher energies is flatter than at lower energies. The fractional amplitude of variability in the frequency range 0.01–1 Hz is also, on average, higher at high energies. As it can be seen in Fig. 7, the *rms* data points measured from the 10-30 keV power spectrum lie systematically above the one-to-one relationship, denoted by the straight line.

Then we investigated the interdependency of the spectral and temporal parameters. Figure 8 shows the relationship between the power-law index resulting from the power spectra using the 2–60 keV (*Standard1*) light curves (Γ_{PSD}) and the photon index from the energy spectra (Γ_{SPEC}). It is clear that in the bright state steeper energy spectra correspond to steeper power spectra. However, this correlation is lost in the faint state.

The variation of the temporal and spectral parameters as a function of the 3–30 keV flux is shown in Fig. 9. Again cor-

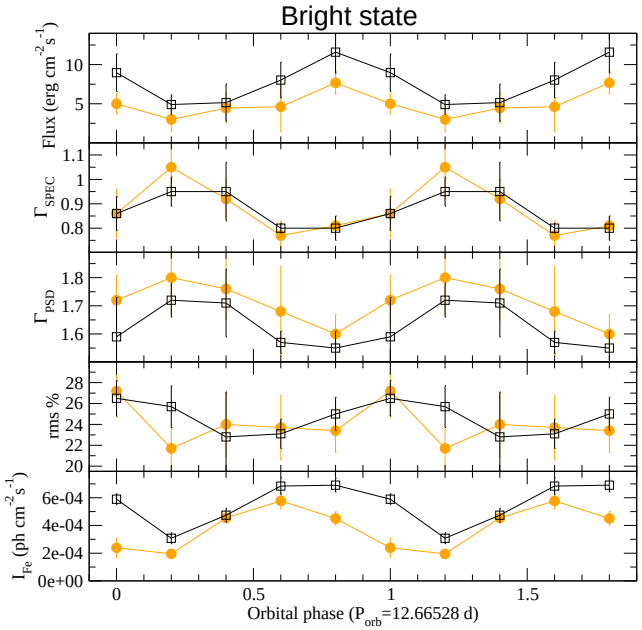

Figure 10. Spectral and timing parameters as a function of orbital phase for the bright state. Circles correspond to state 1 and squares to state 2.

relations between these parameters are apparent in the bright state only. The Γ_{SPEC}-flux plot confirms the known result that the source spectrum becomes harder for higher flux (Baykal et al. 2002; Camero-Arranz et al. 2007). However, we find that this correlation also holds in the timing domain with flatter power spectra being associated with higher flux. The $\Gamma_{SPEC} - \Gamma_{PSD}$ (or Γ_{PSD}-flux) represent new results, not previously reported on a high-mass X-ray binary.

3.5 Orbital phase variability

We also searched for orbital variability in the bright and faint states. We assigned an orbital phase to each PCA observation falling within the four intervals defined in Table 4 using the orbital solution of Camero-Arranz et al. (2007) (no significant difference was found in the results if the orbital parameters of Baykal et al. (2007) were used). The data points were then grouped into five phase bins. Figure 10 shows the results of the orbital variability analysis. We show the bright state only as no correlation with orbital phase was found in the faint state. The X-ray flux in the 3-30 keV band in units of 10^{-10} erg cm^{-2} s^{-1}, the photon index of the energy spectra, Γ_{SPEC}, the power-law index of the power spectra, Γ_{PSD}, the fractional amplitude of variability in the frequency range 0.01–1 Hz, *rms*, and the intensity of the iron line, I_{Fe}, are shown as a function of orbital phase. In this figure, periastron corresponds to orbital phase ∼0.4, while maximum flux is reached around phase 0.7.

When the 3-30 keV flux is high, the intensity of the iron line is also high, while the photon index and power-law index are low. The *rms* also shows a weak modulation: the source appears more variable when the flux is high, but the relatively large errors diminish the significance of this trend. The iron line energy remains fairly constant throughout the orbit. A weighted mean gives 6.44±0.06 keV.

4 DISCUSSION

4.1 Optical analysis

Numerous studies on Be stars (Dachs et al. 1986; Hummel & Vrancken 1995; Hanuschik 1996; Porter & Rivinius 2003; Tycner et al. 2005; Jones et al. 2008) showed that the equatorial disc in Be stars is rotationally supported consistent with a Keplerian velocity field and that the strength and shape of the Hα line provides important information on the structure of the disc. Double-peaked profiles have been interpreted as a result of the Keplerian motion of the particles in the disc, with the peak separation giving an estimate of the rotation velocity. Split profiles are expected to occur when the disc is smaller, that is, at smaller radii. When the disc grows, since the Keplerian velocity is inversely proportional to the radius, the velocity becomes too small to be discernible in low or intermediate resolution spectra. This trend of double-peaked profiles merging in to one single-peak line as the Hα equivalent width increases is a well known result both in Be stars (Dachs et al. 1986) and Be/X (Reig et al. 2000).

We find a good correlation between the strength and shape of the Hα line and the X-ray intensity in SAX J2103.5+4545 (Fig. 2). Emission line profiles are seen only when the source is bright in X-rays, while low-intensity X-ray states are associated with absorption line profiles. This type of correlation has been seen in other Be/X. What makes SAX J2103.5+4545 unique is the rapidity of the changes in the strength and shape of the Hα line, presumably due to a the rapid growth of the disc and the almost immediate transfer of matter into the neutron star to generate X rays. Typically, the time scales for the formation and disappearance of the circumstellar disc in BeX are larger than 3 years (see e.g. Reig et al. 2005). In SAX J2103.5+4545 it is 1–2 years. Thanks to our monitoring in the optical band we can put some constraints on the duration of the formation and subsequent loss of the disc (see Fig. 1 and Table 1). The Hα line was in absorption with EW(Hα)=+2.4 Å without any trace of fill-in emission in June 2006. The largest value of the EW(Hα), which would roughly correspond to the maximum extension of the circumstellar disc, was achieved in September 2007, that is, SAX J2103.5+4545 took about 14 months to develop the circumstellar disk. This duration should be considered as an upper limit. Given the drop in X-ray intensity around January 2007 and the lack of observations in the optical band at this time, it is very likely that the Hα was in absorption at the beginning of 2007. If this is the case then the formation of the disk took just about 8 months. By December 2007, the strength of the Hα line was clearly in the decline, turning into an absorption phase (EW(Hα) had weakened to just 1 Å, although still in emission). Full absorption at a level of EW(Hα)=+2.3 Å was seen about one year after maximum. We conclude that the total duration of the formation/dissipation of the circumstellar disc in SAX J2103.5+4545 is $\lesssim$ 2 yr, and most probably of the order of 1.3–1.5 yr. This duration compares to 3-5 yr of 4U 0115+63 (Reig et al. 2007), 4-5 yr of A 0535+26 (Haigh et al. 2004) and V0332+53 (Goranskii 2001), 4 yr of LS 992 (Reig et al. 2001) and 7 yr of X-Per (Clark et al. 2001). The reason for these fast changes must lie in the relatively narrow orbit (SAX J2103.5+4545 is the Be/X with the shortest orbital period).

In SAX J2103.5+4545 changes in the disc happen so fast that the system does not have the time to develop a large disc. The fact that *i)* the largest EW(Hα) measured in SAX J2103.5+4545 is ∼ -5 Å, a relatively small value and *ii)* the emission line profile appears always as double peaked, provide evidence in support of a small disc radius. The narrow orbit and continuous passages of the

neutron star limit the growth of the disc and do not allow the Be star to develop an extended disc. On the other hand, the duration of the disc-loss phase also seems to be short. In fact, it is likely that the complete loss of the disc never materialises. An inspection of Table 1 reveals that CQE and emission profiles are present in the majority of the observations. As stated above emission lines are formed in the disc. CQE profiles also require that a circumstellar disc exists, although of a much smaller spatial extent (Rivinus et al. 1999). Note also that some of the profiles classed as pure absorption may contain a weak central peak that is not apparent due to the low spectral resolution. Another interesting characteristic of the X-ray behaviour of SAX J2103.5+4545 is the large and sudden increase in intensity that precedes some of the outbursts. The X-ray intensity increases by a factor of ∼20 in a few days. The onset of these flares occurs at or near periastron and last for no more than two or three orbital cycles. Then the X-ray intensity abruptly falls to almost pre-flare values. Immediately after, a lower intensity and longer outburst begins (the bright state).

Thus the picture that emerges to explain the long-term X-ray/optical variability is the following: the Be star's equatorial disc forms due to ejections of matter from the Be star's photosphere through a still unknown mechanism. As the disc grows the Hα line turns from absorption into emission. The fact that the emission line profile is always split, i.e., no single-peak line is seen and the relatively small EW(Hα) indicates a small disc. We can estimate the disc radius from the separation of the Hα profile peaks, as this value and the outer radius ($R_{\rm disc}$) of the emission line forming region are related by (see e.g. Hummel & Vrancken 1995)

$$\frac{R_{\rm disc}}{R_*} = \left(\frac{2v\sin i}{\Delta_{\rm peak}}\right)^2 \quad (1)$$

where $v \sin i$ is the projected rotational velocity of the B star (v is the equatorial rotational velocity and i the inclination toward the observer). For SAX J2103.5+4545 $v \sin i \approx 240$ km s^{-1} (Reig et al. 2004), while the average peak separation, as measured from the September 2007 spectra is $\Delta_{\rm peak} = 340$ km s^{-1}. Thus R$_{\rm disc}$ $\sim 2-3$ R$_*$. Taking the characteristic values of mass and radius of a B0 star, namely $M_* = 20$ M$_\odot$ and $R_* = 8$ R$_\odot$ for the B star (Vacca et al. 1996) and the canonical mass of a neutron star $M_x = 1.4$ M$_\odot$, the orbital period ($P_{\rm orb} = 12.6$ d) implies, according to Kepler's third law, an orbital separation of $a \approx 63$ R$_\odot$ or equivalently $a \approx 8\ R_*$. Correspondingly, periastron lies at $R_{\rm per} = 4.7\ R_*$ for an eccentricity $e = 0.4$. Similarly, the radius of the Roche lobe of the primary star is (Paczyński 1971) $R_{RL}/a = 0.38+0.20\log(M_*/M_x) = 0.6$. That is, the radius of the disc is similar to the size of the Roche lobe, which in turn, is similar to the periastron distance, $R_{RL} \approx R_{\rm per} \sim R_{\rm disc}$.

We conclude that due to the small orbit, the neutron star truncates the disc at very small radii. It is very likely that, occasionally, the neutron star physically impinges on the disc during periastron passage giving rise to sharp and intense X-ray flares. Note that the fact that $R_{\rm disc} = 2\,R_*$ does not mean that the disc terminates abruptly at that distance, but matter would extend to larger radii following a density law of the form $\rho \sim r^{-\beta}$, where $\beta \approx 2.5-3$ (Waters 1986, 1988). The fact that the optical indicators (magnitudes and EW(Hα)) continue rising after the flare episode implies that the disc has not yet been destroyed. In subsequent periastron passages, matter is still transferred to the neutron star but in a less dramatic way. An accretion disc around the neutron star is likely to be formed, as indicated by the spin-up episodes (Inam et al. 2004; Camero-Arranz et al. 2007). When the fuel that power the X-ray activity is used up, that is to say, when the circumstellar disc disappears then accretion ceases and the source returns to an X-ray quiescent state.

4.2 X-ray analysis

Our X-ray spectral analysis of the bright and faint states of SAX J2103.5+4545 confirms previous reports (Baykal et al. 2002, 2007; Camero-Arranz et al. 2007) that in the bright state the spectrum is harder than in the faint state. This result is opposite to what it is seen in other types of X-ray binaries but it is not exclusive of SAX J2103.5+4545. Black-hole systems and low-mass X-ray binaries display different source states (van der Klis 2006, and references therein). In black-hole systems three basic states are identified, namely, soft, hard and intermediate (which includes the so called very high state). Although these states may occur at any luminosity, when the black-hole system is followed through an outburst, the soft state normally corresponds to higher X-ray intensity values, while the hard state is normally seen at the beginning and end of the outburst, i.e, at lower count rates. Likewise, spectrally hard states in low-mass X-ray binaries occur at lower luminosities than softer spectra states (Olive et al. 2003; Maccarone & Coppi 2003). In contrast, in a spectral and timing study of four Be/X-ray during major outbursts, Reig (2008) found that three of the sources investigated showed low/soft spectral states (the so-called horizontal branch) at the beginning and at the end of the outburst.

The origin of these differences must lie on the accretion processes in the vicinity of the compact object. Unlike black-hole systems and low-mass X-ray binaries with weak magnetic-field neutron stars, the compact object in Be/X-ray binaries is a strongly magnetised neutron star, which results in significant coupling of the magnetic field and the accretion flow (White et al. 1983). One of the results of this coupling is that the accretion flow is threaded onto the neutron star magnetic field lines and channeled on to the magnetic poles, producing two or more localised X-ray hot spots (see e.g Frank et al. 2002). Above these hot spots the magnetic field lines adopt the configuration of a roughly column-shaped surface or funnel, which is referred to as the accretion column, the polar cap being its base. The polar caps are treated as dense thermal mounds with a blackbody spectrum. The detection of such blackbody components at low energies in a number of low-luminosity X-ray pulsars give support to the existence of such thermal mounds (Coburn et al. 2001; Mukherjee & Paul 2005; La Palombara & Mereghetti 2006; Reig et al. 2009). The surface of the mound is responsible for photon creation and absorption (Becker & Wolff 2005). The high-energy emission observed from accreting pulsars results from the formation of a standing shock wave on this accretion column: the energetic particles in the accretion flow comptonise the thermal emission produced on the polar cap (Becker & Wolff 2005). Increased mass accretion rates are expected to result in harder X-ray spectra (Langer & Rappaport 1982; Becker & Wolff 2005) because the photons spend more time, on average, being upscattered in the flow before escaping.

The faint state corresponds to a quiescence and stable state of the source in which the X-rays are no longer powered by disc accretion but most likely are the result of wind accretion. Wind-fed system, like supergiant X-ray binaries, show erratic and flaring (high-amplitude changes on timescales of seconds) X-ray variability that it is consequence of inhomogeneities in the accretion wind. This type of variability is almost absent in SAX J2103.5+4545, where the main source of variability at short timescales are the X-ray pulsations. The fact that we do not see random high-amplitude variations during the faint state of SAX J2103.5+4545 might in-

dicate that the dominant accretion wind is the more stable equatorial low-velocity high-density wind characteristic of BeX (Waters 1988). This wind, that ultimately would create the circumstellar disc, would be highly suppressed during the faint state. It would also indicate that the neutron star orbit is coplanar to the plane of the circumstellar disc. Otherwise, the neutron star would be exposed to the higher velocity and more inhomogeneous polar winds, typical of massive stars, giving rise to erratic X-ray variability. The narrow orbit of SAX J2103.5+4545 would also help avoid the polar winds if the orbit is coplanar to the disc. Occasionally sudden and short-lived increases in X-ray flux are seen superimposed on a long-term decline phase during the faint state (see e.g. MJD 52800–53200 in Fig. 4). These mini-outbursts may correspond to fail attempts to create the circumstellar disc, i.e. ejection of matter from the Be star's photosphere that are not retained by the star.

In contrast, the bright state exhibits high richness in variability. Both spectral and temporal parameters correlate with one another and with X-ray flux and orbital phase. During the orbital maximum the spectral photon index is minimum. Similar variability behaviour has been reported in the supergiant X-ray binary 2S 0114+650 (Farrell et al. 2008). Based on the similarities with the eclipsing X-ray pulsar EXO 1722–363 (Thompson et al. 2007), Farrell et al. (2008) attributed the spectral variability to absorption effects as the neutron star passes behind a heavily absorbing wind.

We have found for the first time in a HMXB a correlation between the shape of the energy and power spectra, namely softer energy spectra correspond to the disappearance of power at high frequencies, i.e. softer power spectra. Although there are no detailed models of the power spectra arising from accretion onto highly magnetized neutron stars, one would expect that the simple scenario described above would also explain the $\Gamma_{\rm SPEC} - \Gamma_{\rm PSD}$ correlation (Fig. 8) At high mass accretion rates, i.e., when the X-ray flux is high, the magnetosphere shrinks, as the magnetosphere's radius $r_{\rm m} \propto \dot{M}^{-2/7}$ (see e.g. Davidson & Ostriker 1973). If the source of variability in the power spectrum comes from the interaction between the accretion disc and the magnetosphere then smaller magnetospheric radius implies shorter characteristic time scales (or higher frequencies), hence flatter power spectra. When the flux decreases (softer energy spectrum), the size of the magnetosphere increases and so does the characteristic timescale of variability producing more power at low frequencies, hence steeper power spectra. The fact that the *rms* is similar in the bright and faint states supports the notion that the source of variability is similar in both states and the only difference is the size of the emitting region.

If we assume that the characteristic frequencies result from Keplerian motion in the inner parts of the accretion disc, and that the accretion disc extends all the way down to the magnetosphere, then the characteristic Keplerian frequency of an orbiting free particle is

$$\nu = \sqrt{\frac{GM}{4\pi^2 r_{\rm m}^3}}$$

Assuming that all the kinetic energy of infalling matter is given up to radiation, i.e., $L_{\rm x} = GM_{\rm x}\dot{M}/R_{\rm x}$, an increase of the X-ray luminosity by a factor of ∼6, as observed in the bright state of SAX J2103.5+4545, implies a reduction in the size of the magnetosphere by ∼ 40%, while the characteristic frequency of variability increases by a factor ∼2.

In Fig. 7 we showed that the fractional *rms* is larger at higher energy. If the source of variability were variations in the soft photon input, then simple Comptonization models would predict a decrease of the amplitude of variability with increasing photon energy. This trend is the result of the averaging effect of Compton scatterings: low-energy photons retain most of the variability of the seed photon input because they have not suffered many scatterings. In contrast, the variability of high-energy photons is smeared out as these photons spend longer time in the comptonizing medium. These prediction are not consistent with observations of black-hole systems. In low-mass X-ray binaries and black-hole systems, the fractional *rms* of discrete noise components (i.e. QPO) tend to increase with photon energy (Gilfanov et al. 2003; Homan et al. 2001). In the case of broad-band noise, the relationship of the *rms* with energy shows a much more complex behaviour (Lin et al. 2000), and it is source state dependent (Gierliński & Zdziarski 2005). Note also that in black-hole binaries the geometry of the Comptonizing medium is very different from the geometry in the pulsar accretion column and the optical depth is expected to be lower. In order to have larger fractional *rms* at higher energies, as shown in Fig 7, the source of variability cannot be solely due to intrinsic variations of the source of soft photons. Gierliński & Zdziarski (2005) found that an increase in the fractional *rms* with photon energy can be achieved if the power released in the comptonising plasma changes, i.e., if the energy of the comptonising electrons changes (electron acceleration and/or direct heating). Applied to SAX J2103.5+4545 this would mean that the power supplied to the electrons in the accretion flow changes, perhaps as a result of varying mass accretion rate, which may well affect the geometry and optical depth of the Comptonizing column.

5 CONCLUSIONS

We have performed an analysis of the X-ray timing and spectral properties of the Be/X-ray binary SAX J2103.5+4545 in correlation with optical spectroscopic observations of the Hα line. We find a good correlation between the strength and profile of this line and the X-ray activity of the source. Emission line profiles are observed during bright X-ray states. In these states the Hα equivalent width is largest. During faint X-ray states Hα appears in absorption. SAX J2103.5+4545 exhibits the fastest time scales for the disappearance and reformation of the circumstellar disc, compared to other typical Be/X-ray binaries. In less than 2 years SAX J2103.5+4545 is capable to form and lose the disc. Due to its narrow orbit, the neutron star prevents the disc from extending to large radii; the disc is truncated at 2–3 stellar radii. Based on the Hα line profile we set stringent constraints on the size of the circumstellar disc and we find that its size can reach the Roche-lobe radius of the system (which it is similar to the periastron distance of the two objects).

We have also performed for the first time in a Be/X-ray binary a correlated study of the X-ray spectral and timing properties and found a correlation between the shape of the energy spectrum and that of the power spectrum in the bright state. When the energy spectrum is soft, the power at high frequencies is suppressed. This correlation, together with the existence of hard/high and soft/low states, has been interpreted in the context of emission from the accretion column.

ACKNOWLEDGMENTS

We thank all the observers that helped obtain the optical spectra: P. Berlind and M. Calkins from FLW observatory and A. Manousakis, M. Lanzara, E. Beklen, and E. Nespoli from the SKI observatory. This work has been supported in part by the European Union

Marie Curie grant MTKD-CT-2006-039965 and EU FP7 "Capacities" GA No206469. A. Słowikowska is partially supported by the Polish Ministry of Science and Higher Education project 362/1/N-INTEGRAL (2009-2012). This work has made use of NASA's Astrophysics Data System Bibliographic Services and of the SIMBAD database, operated at the CDS, Strasbourg, France. The ASM light curve was obtained from the quick-look results provided by the *RXTE*/ASM team. *SWIFT*/BAT transient monitor results provided by the *SWIFT*/BAT team. Skinakas Observatory is a collaborative project of the University of Crete, the Foundation for Research and Technology-Hellas and the Max-Planck-Institut für Extraterrestrische Physik.

REFERENCES

Barthelmy, S. D., 2000 on behalf of the Swift Instrument Team, SPIE, vol 4140, pp 50.
Baykal, A., Stark, M.J., & Swank, J.H., 2000, ApJ, 544, 129
Baykal, A., Stark, M.J., & Swank, J.H., 2002, ApJ, 569, 903
Baykal, A., Inam, S.,Ç., Stark, M.J., et al. 2007, MNRAS, 374, 1108
Becker P. A., Wolff M. T., 2005, ApJ, 630, 465
Belloni, T., & Hasinger, G. 1990, 230, 103
Blay, P., Reig, P., Martnez Nnez, S., et al. 2004, A&A, 427, 293
Camero Arranz, A., Wilson, C. A., Finger, M. H., Reglero, V., 2007, A&A, 473, 551
Clark, J. S., Tarasov, A. E., Okazaki, A. T., Roche, P., Lyuty, V. M. 2001, 380, 615
Coburn, W., Heindl, W. A., Gruber, D. E., et al. 2001, ApJ, 552, 738
Corbet, R. H. D., 1986, MNRAS, 220, 1047
Dachs, J., Hanuschik, R.W., Kaiser, D., Rohe, D., 1986, A&A, 159, 276
Dachs, J., Hummel, W.;, & Hanuschik, R. W., 1992, A&AS, 95, 437
Davidson, K. & Ostriker, J.P., 1973, ApJ, 179, 599
Dougherty, S. M., Waters, L.B.F.M., Burki, G., et al., 1994, A&A, 290, 609
Fabricant, D., Cheimets, P., Caldwell, N., & Geary, J. 1998, PASP, 110, 79
Farrell, S.A., Sood, R.K., O'Neill, P.M., & Dieters, S., 2008, MNRAS, 389, 608
Ferrigno, C., Segreto, A., Santangelo, A. et al. 2007, A&A, 462, 995
Frank J., King A., Raine D. J., 2002, in *Accretion Power in Astrophysics*, Cambridge University Press, ISBN 0521620538
Gierliński, M. & Zdziarski, A.A., 2005, MNRAS, 363, 1349
Gilfanov, M., Revnivtsev, M., & Molkov, S., 2003, A&A, 410, 217
Goranskii, V. P. 2001, AstL, 27, 516
Grundstrom, E.D. & Gies, D.R. 2006, ApJ, 651, L53
Gutiérrez-Moreno, A., 1979, PASP, 91, 299
Haigh, N. J., Coe, M. J., Fabregat, J. 2004, MNRAS, 350, 1457
Hanuschik, R.W., 1995, A&A, 295, 423
Hanuschik, R.W., 1996, A&A, 308, 170
Homan, J., Wijnands, R. & van der Klis, M., et al. 2001, ApJS, 132, 377
Hulleman, F., in 't Zand, J.J.M., & Heise, J., 1998, A&A, 337, L25
Hummel, W., & Vrancken, M., 1995, A&A, 302, 751
Inam, S.Ç, Baykal, A., Swank, J. & Stark, M.J. 2004, ApJ, 616, 463
Jahoda K., Swank J.H., Stark M.J., Strohmayer T., Zhang W., Morgan E.H., 1996 *EUV, X-ray and Gamma-ray Instrumentation for Space Astronomy VII*, O.H.W. Siegmund & M.A. Gummin eds., SPIE 2808, 59, 1996.
Jaschek, C. & Gómez, A.E., 1998, A&A, 330, 619
Jones, C.E., Sigut, T.A.A., Porter, J.M., 2008, MNRAS, 386, 1922
Johnson, H. 1966 ARA&A, 4, 193
Lebrun, F., Leray J.P., Lavocat, P., et al. 2003, A&A, 411, 141
Langer S. H., Rappaport S., 1982, ApJ, 257, 733
Landolt, A.U., 2009, AJ, 137, 4186
La Palombara, N., & Mereghetti, S. 2006, A&A, 455, 283
Levine, A.M., Bradt, H., Cui, W., et al. 1996, ApJ, 469, L33
Lin, D., Smith, I.A., Bttcher, M., & Liang, E.P., 2000, ApJ, 531, 963
Maccarone, T.J. & Coppi, P.S., 2003, A&A, 399, 1151
Miyamoto, S., Kimura, K., Kitamoto, S., Dotani, T., Ebisawa, K. 1991, ApJ, 383, 784
Mukherjee, U., & Paul, B. 2005, A&A, 431, 667
Olive, J., Barret, D. Gierlinski, M. 2003, ApJ, 583, 416
Paczyński, B, 1971, ARA&A, 9, 183
Porter, J.M. & Rivinius, T., 2003, PASP, 115, 1153
Reig, P., & Roche, P. 1999, MNRAS, 306, 100
Reig, P., Negueruela, I., Coe, M. J., et al., 2000, MNRAS, 317, 205
Reig, P., Negueruela, I., Buckley, D. A. H., Coe, M. J., Fabregat, J., Haigh, N. J. 2001, A&A, 367, 266
Reig, P., Negueruela, I., Fabregat, J., et al. 2004, A&A, 421, 673
Reig, P., Negueruela, I., Papamastorakis, G., Manousakis, A., Kougentakis, T. 2005, A&A, 440, 637
Reig, P., Larionov, V., Negueruela, I., Arkharov, A. A., & Kudryavtseva, N. A., 2007, A&A, 462, 1081
Reig, P., 2008, A&A, 489, 725
Reig, P., Torrejn, J. M., Negueruela, I., et al., 2009, A&A, 494, 1073
Rivinus, T., Stefl, S. & Baade, D., 1999, A&A, 348, 831
Rothschild, R.E., Blanco, P.R., Gruber, D.E., et al. 1998, ApJ, 496, 538
Sidoli, L., Mereghetti, S., Larsson, S., et al. 2005, A&A, 440, 1033
Thompson, T.W.J., Tomsick, J.A., in 't Zand, J.J.M., Rothschild, R.E., & Walter, R. 2007, ApJ, 661, 447
Tokarz, S. P., & Roll, J. 1997, Astronomical Data Analysis Software and Systems VI, 125, 140
Tycner, C., Lester, J.B., Hajian, A.R., et al. 2005, ApJ, 624, 359
Vacca, W. D., Garmany, C. D., & Shull, J. M., 1996, ApJ, 460, 914
van der Klis, M. 2006, in *Compact Stellar X-ray sources*, eds. W.H.G. Lewin & M. van der Klis, Cambridge University Press, p.39
Waters, L.B.F.M., 1986, A&A, 162, 121
Waters, L.B.F.M., van den Heuvel, E.P.J., Taylor, A.R., Habets, G.M.H.J., & Persi, P., 1988, A&A, 198, 200
Wegner, W., 1994, MNRAS, 270, 229
Wegner, W., 2006, MNRAS, 371, 185
White N. E., Swank J. H., Holt S. S., 1983, ApJ, 270, 711